Journal of Materials Chemistry C

Accepted Manuscript

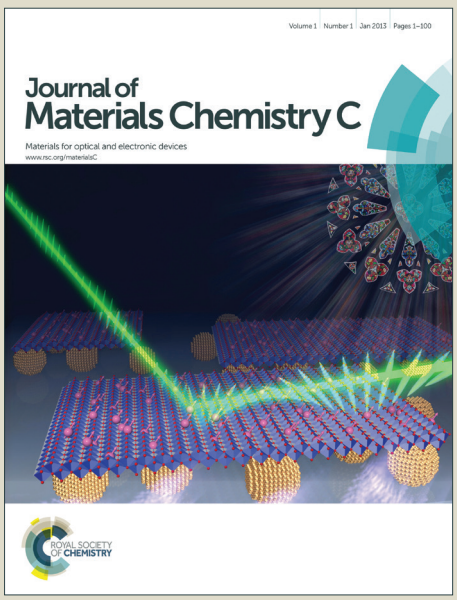

ROYAL SOCIETY OF CHEMISTRY

www.rsc.org/materialsC

A prominent dielectric material with extremely high-temperature and reversible phase transition in the high thermally stable perovskite-like architecture

Fang-Fang Wang, Cheng Chen, Yi Zhang, Heng-Yun Ye, Qiong Ye*, Da-Wei Fu*

Ordered Matter Science Research Center, Southeast University, Nanjing 211189, P.R. China

Abstract: One perovskite-like dielectric material $(C_3N_2H_5)\cdot[Mn(HCOO)_3]$ (**1**), exhibiting remarkably high T_c (phase transition temperature) and pronounced dielectric anomaly, can be considered as a model of novel extremely high-temperature dielectric materials. The systematic characterizations, including detailed differential scanning calorimetry (DSC), variable-temperature single crystal X-ray and X-ray powder diffraction analyses, variable-temperature IR spectra as well as temperature-dependence and frequency-dependence dielectric measurements, reveal a sharp structural phase transition from tetragonal $P\text{-}42_1m$ at HTP (high temperature phase) to monoclinic $P2_1/c$ at RTP (room temperature phase) and the mechanism of dielectric and thermal anomalies can be ascribed to the host-guest interaction coupled with the order-disorder transitions of the $Mn(HCOO)_3^-$ cage and the $[(C_3N_2H_5)]^+$ guest, which is the result of synergistic effect. Emphatically, the T_c (438K) is the highest one reported so far for a molecule-based dielectric material (the T_c is below room temperature for the most known formate series perovskite-like dielectrics), which makes **1** a promising candidate for molecule-based dramatically high-temperature dielectric materials and may open up new possibilities to make a large breakthrough in the potential practical applications in sensing, dielectric devices, energy storage, data storage and molecular or flexible multifunctional electronic devices.

*E-mail: dawei@seu.edu.cn, yeqiong@seu.edu.cn

.

Introduction

Molecule-based dielectric materials are highly desirable for their easy and environmentally friendly processing, light weight, adjustable structures and properties and mechanical flexibility. Therefore, the materials of metal-organic frameworks (MOFs) with versatile functionalities are vastly investigated in view of their intriguing potential applications in electrically controllable microwave elements, data storages, signal processing, switchable dielectric devices, magnetic-field sensor and spintronics devices.[1-2] Among these, the prospects for MOF systems with solid-solid structural phase transition and molecular dielectric behavior, most of which have found practical and high-technological applications, are particularly attractive.[3-8] Besides, the organic ligands employed mainly include the monoatomic I^-, diatomic CN^-, and multiatomic $HCOO^-$, N_3^- anions, which usually act as monovalent end- to-end bridging ligands.[9-11]

According to these principles, ammonium metal-formate frameworks (hereafter abbr. AMFFs) in which the induced order-disorder change of the ammonium cationic guest in the well-matched cage-like frameworks can often be the dominant driving force for structural phase transitions, as observed in many other systems including ammonium components, have been systematically studied, and to date, numerous interesting results and developments for AMFFs have been covered.[12-18] Compared with conventional pure inorganic or organic compounds, AMFFs taking advantage of structural malleability and modulation to develop polarizable molecular materials could display a variety of physical properties and critical phenomena or phase transitions.[5] Especially, the formate $HCOO^-$, which is the smallest and simplest carboxylate, can link to metal ions to construct the cages by multifarious bridging modes and fortunately, there is still much room and possibility for the integration of flexible units into the cages. Usually, scientists introduced the polarizable species, for example imidazolium,[19-21] into the well-matched molecular-based phase transition compounds and the delicate match of the components, upon external stimuli like

temperature and pressure, becomes instable to bring about a structural reorganization.[22-27]

From an application point of view, finding materials that exhibit phase transition at high temperature or as close as possible to room temperature is extremely significant. Namely, the fact that in the compounds dielectric transition occurs below room temperature imposes important restrictions on potential practical applications. However, **1**[28-29] exhibits interesting structural phase transition with T_c as high as 438 K. Particularly, the compound that displays transition at such a high critical temperature is comparatively rare. Previously reported AMFFs usually show low T_c, such as $[NH_4]\cdot[Mg(HCOO)_3]$, T_c = 255 K,[13] $[(CH_3)_2NH_2]\cdot[Mn(HCOO)_3]$ (T_c = 187 K),[16] and $[NH_2NH_3]\cdot[Mg(HCOO)_3]$ (T_c = 348 K).[14] In fact, the high phase transition temperature of **1** is exactly comparable to those of a typical inorganic ceramic ferroelectric $BaTiO_3$ (T_c = 393 K)[30] and some molecular ferroelectrics, such as [Hdbco] ClO_4 (bdco = 1, 4- diaza- bicycle [2.2.2.] octane, T_c = 393 K),[31-32] triglycine fluoberyllate (TGFB, T_c = 352 K),[33] and diisopropylammonium chloride (T_c = 440 K).[34]

This perovskite-like compound $(C_3N_2H_5)\cdot[Mn(HCOO)_3]$ presents an extremely high-temperature phase transition at approximately 438 K far below the melting point, characterized systematically by DSC, variable-temperature X-ray powder diffraction (XRPD), variable-temperature single crystal X-ray diffraction, variable-temperature IR spectra, and temperature-dependent and frequency-dependent dielectric measurements. Here, the structures at different temperatures are analyzed thoroughly and discussed deeply to discover and elucidate the origin of structural phase transition. The Mn (II) ions bridged by the formate in an anti-anti mode of coordination fabricate the cage host, and the counter-balanced imidazolium cation guest resides in the interstitial void of the well-designed framework through rich hydrogen bonds. Besides, the dielectric properties around the T_c are investigated elaborately. Obviously, the mechanism of dielectric and thermal anomalies can be ascribed to the abrupt order-disorder transform of imidazolium cation and a subsequent successive displacement and significant rotation for both the $HCOO^-$ groups and the

octahedraon-like MnO_6. Emphatically, because of its extremely high critical temperature (438K), the highest T_c reported so far for formate series perovskite-like molecular dielectric materials, the present compound **1** may be a fascinating candidate for molecular-based extremely high-temperature dielectric materials. Therefore, our work may open up new approaches to break through the potential practical applications in sensing, dielectric devices, energy storage, data storage, electro-optics, and molecular or flexible multifunctional electronic devices.

Experimental section

Synthesis. In this work, chemicals and solvents were commercially obtained as chemically pure and used without any further purification. Compound **1** was prepared through conventional solution method. A methanol solution (6mL) of 6.4mmol imidazole and 9.6mmol formic acid was placed in a glass tube. Upon this solution, 2mL of methanol was carefully added, followed by carefully layering 4mL of methanol solution containing 0.80mmol $Mn(ClO_4)_2 \cdot 6H_2O$. Subsequently, the tube was sealed and kept undisturbed. After two days, colorless, block-shaped, X-ray quality crystals were obtained.

Single crystal X-ray crystallography. X-ray diffraction data of **1** were collected with Mo *Kα* radiation (λ = 0.71073 Å) on a Rigaku SCXmini diffractometer using the ω scan technique at 293(2) K and 453(2) K. Cell parameters were retrieved and refined using CrystalClear software on all observed reflections. The structures of **1** at different temperatures were solved by the direct methods and refined by full-matrix least squares methods on F^2 in SHELXL program package. All non- hydrogen atoms were refined anisotropically using all reflections with $I > 2\sigma(I)$, while all H atoms were positioned geometrically and refined using a "riding" model for aromatic ring H atoms with $U_{iso} = 1.2\ U_{eq}$ (C), methyl H atoms with $U_{iso} = 1.5\ U_{eq}$ (C), and ammonium H atoms with $U_{iso} = 1.5\ U_{eq}$ (N). Details about the data collection and refinement of the RTP and HTP are summarized in Table 1. Besides, further details are provided in the supplementary material（Table S1）. Asymmetric units and the packing views were

all drawn with DIAMOND Visual Crystal Structure Information System Software. Distances and angles between some atoms were calculated using DIAMOND, while other calculations were carried out using SHELXLTL.

Table 1 Crystal data and structure refinement for **1** at 293 K and 453 K

	RTP (293K)	HTP (453K)
Empirical formula	$C_6H_8MnN_2O_6$	$C_6H_8MnN_2O_6$
Formula weight	259.08	259.08
Temperature (K)	293(2)	453(2)
Crystal system	Monoclinic	Tetragonal
Space group	$P2_1/c$	$P\text{-}42_1m$
a/ Å	12.345(7)	8.8169(10)
b/ Å	12.481(7)	8.8169(10)
c/ Å	17.627(3)	6.4562(12)
β/ deg	133.15(2)	90
Volume ($Å^3$)	1981.4(1)	501.89(12)
Z	8	2
Calculated density (g cm^{-3})	1.737	1.714
Absorption coefficient (mm^{-1})	1.344	1.326
F(000)	1048	262
θ range for data collection	2.26–27.50°	3.91–27.45°
Limiting indices	$-15 \le h \le 16$	$-7 \le h \le 8$
	$-15 \le k \le 16$	$-6 \le k \le 11$
	$-22 \le l \le 16$	$-7 \le l \le 8$
Reflections collected / unique	13814 / 4489	1747 / 374
R (int)	0.0321	0.1150
Completeness to *θ* (%)	98.7	98.0
Data / restraints / parameters	4489 / 0 / 279	293 / 30 / 48
Goodness-of-fit on F^2	1.156	1.287
$R_1/wR_2[I > 2\sigma(I)]$	0.0415/ 0.1115	0.0823/ 0.1906
R_1/wR_2 (all data)	0.0622/ 0.1295	0.1068/ 0.2053
Larg. peak/hole (e $Å^{-3}$)	0.558/ −0.431	1.159/ -0.477

DSC and TGA measurement. DSC runs were recorded on a Rigaku DSC8230 instrument, upon heating and cooling microcrystalline samples of 9.1 mg weight at a rate of 10 K/ min in aluminum crucibles at atmospheric pressure. Besides, to investigate the thermal stability of **1**, thermal gravimetric analysis (TGA) and DSC of

1 were performed with a heating rate of 10 K min^{-1} under nitrogen atmosphere in the temperature range of 363- 913 K.

Variable- temperature IR spectra, Solid- state UV-Vis reflectance spectra, and X-ray powder diffraction. Powder infrared spectra of the title crystals in the temperature range of 293-463 K were measured with the Spectrum 100 over the wavenumber range 4000-450 cm^{-1} (Fig. S1). Besides, the solid- state UV-vis reflectance spectrum (Fig S2) of **1** was also measured. X-ray powder diffraction measurements were made with a Rigaku/ D-MAX diffraction system, equipped with a copper X-ray tube $\lambda_{Cu\text{-}K\alpha}$ = 1.5406 Å and a graphite monochromator. The powder patterns reported are the result of addition of three single scan patterns from 2θ = 5º to 2θ = 50º at 5º/min with an increment of 0.02º. The XRPD pattern of **1** at room temperature matches very well with the pattern simulated from the single-crystal structure, which indicates the phase purity of **1** (Fig. S3). Because of the different powder size during collection of the experimental XRPD data, there are some differences in reflection intensities between the simulated and experimental patterns.

Dielectric measurements. The complex dielectric constant ε ($\varepsilon = \varepsilon' - i\varepsilon''$) was measured on a Tonghui TH2828A in the frequency range between 1 KHz and 1 MHz, from 300 to 480 K, applying an AC voltage of 1 V. Because it is hard to obtain large size crystals, the dielectric studies (capacitance and dielectric-loss measurements) were performed on powder samples which had been pressed into tablets, on the surfaces of which conducting silver glue was deposited, that is to simulate a parallel plate capacitor.

Results and discussion

Phase transition of 1.

DSC measurement is an extremely effective approach to detect whether the compound exhibits a distinguished reversible structural phase transition during the heating and cooling processes in response to external temperature stimulus or not, and the DSC measurement of **1** accomplished in the temperature range of 303-573 K

evidences the existence of the phase transition behavior. The obtained curves which are absolutely reproducible can display clearly an endothermic peak upon heating at approximately 438.0 K and the homologous exothermic peak at around 434.3 K (Fig. 1(a)), representing a prominent and reversible phase transition at T_c = 438.0 K with a small thermal hysteresis of 3.7 K. The phase transition temperature of 438.0 K upon heating is very in good accordance with the DSC data reported in the literature.[28-29] Particularly, the compound that displays phase transition at such a high critical temperature is comparatively rare. The combined round shape of the anomalous peaks and relatively small thermal hysteresis (3.7 K) clearly reveal the continuous characteristic of the phase transition, effectively indicating the presence of a phase transition as a second-order transition.

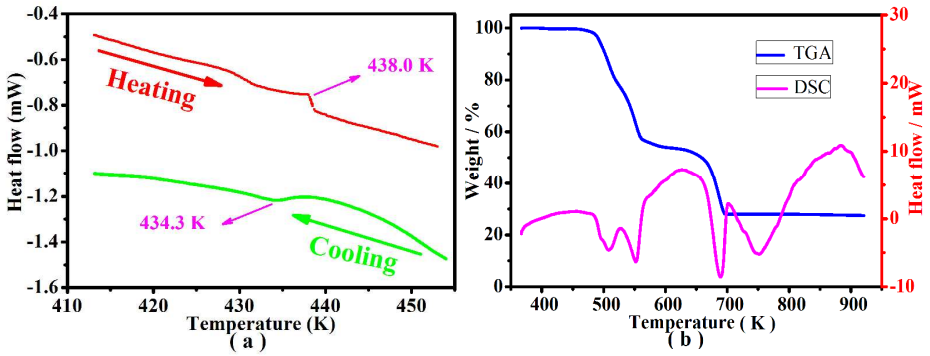

Fig. 1(a) DSC curves of the polycrystals of **1**. Fig. 1(b) TGA and DSC curves of **1** in the temperature range of 363- 913 K.

As plotted in Fig 1(a), an enthalpy change of ΔH_h = 0.103 J g^{-1} and an entropy change of $\Delta S_h = 2.351 \times 10^{-4}$J (g K)$^{-1}$ = 6.090×10^{-2}J (K mol)$^{-1}$ are computed for the heating process, whereas an enthalpy change of ΔH_c = 0.103 J g^{-1} and an entropy change of $\Delta S_c = 2.326 \times 10^{-4}$J (g K)$^{-1}$ = 8.512×10^{-2}J (K mol)$^{-1}$ are calculated for the cooling process. The averaged ΔS for ΔS_h and ΔS_c is *ca.* 7.301×10^{-2}J (K mol)$^{-1}$. An estimation of the number of the molecular orientations from the calorimetric data can be made from the Boltzmann equation, $\Delta S = nR\ln(N)$, where n represents the number of guest molecules per mole, R is the gas constant, and N stands for the ratio of numbers of possible orientations for the disorder system. It is found that N = 1.10, reflecting that the phase transition is a complicated transition rather than a typical

order- disorder transition and is probably related to the change in reorientational dynamics of the imidazolium cation.

Thermal stability of the samples might be exceedingly important for some potential applications especially in some extreme conditions, and might provide some clues on molecule-based dielectric materials. Therefore, TGA of **1** was measured in the temperature range of 363- 913 K (Fig. 1(b)) and it can sufficiently indicate that **1** is relatively stable from the thermal perspective and that the melting point (480 K) is far above the phase transition temperature, which may be highly useful and meaningful in the potential practical applications.

As depicted in the Fig. 1(b), the TGA graph of **1** exhibit three clear weight loss steps. It can be seen that around 470 K, the weight loss may be assigned to the removal of one imidazolium per formula unit in the sample (found 26.57%, calculated 26.67%). The second step of weight loss happens between 510 and 550 K, which is caused by the loss of one formic acid per formula unit (found 17.47%, calculated 17.38%). The last mass loss event that is attributed to a decomposition process at temperatures between 620 and 690 K is consisting with a decomposition of $Mn(HCOO)_2$ to a supposed MnO residue (found 28.53%, calculated 28.58%). Besides, The DSC curve corresponds well to the TGA curve, showing four endothermic peaks during the process of the decomposition of **1**.

In addition, variable-temperature XRPD measurements were performed on polycrystalline samples of **1** to further verify that **1** experiences an obvious structural phase transition within the temperature range of 298- 463 K (Fig. 2). Upon heating, all of the present diffraction peaks at 433 K are nearly consistent with those found at 298 K, that is, RTP. However, above 443 K, the diffraction peaks at 20.18° and 28.64° disappeared, and this may be related to a slight variation of the crystal structure, corresponding to the HTP. Generally, the sharp reduction of the number of diffraction peaks indicates a transition from low symmetry to high symmetry. As expected, these results exhibit obvious phase transition, which is agree well with the DSC measurement.

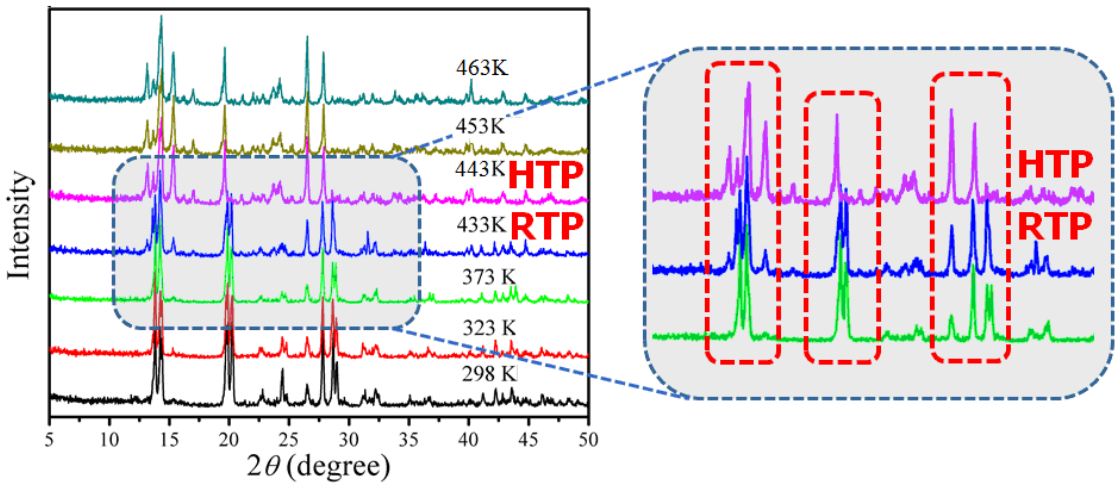

Fig. 2 X- ray powder diffraction (XRPD) patterns obtained at different temperatures between room temperature and 463K.

Crystal structures, structural transitions and mechanism.

To identify if this phase transition is accompanied with a structural alteration, the crystal structures of **1** were obtained and resolved at 293 K and 453 K, respectively. To elucidate the structural change between the two temperatures, the phase at 293 K is named as the RTP and the phase at 453 K is labeled as the HTP for forthcoming comparative investigation. The crystal structures of **1** in both phases can be roughly described as distorted perovskite- like structures, in keeping with a general formula of ABY_3 (the valence ratio of the cationic A, B and anionic Y components is 1:2:1). Variable-temperature X-ray single-crystal diffraction analysis uncovers that **1** crystallizes in the centrosymmetric space group $P2_1/c$ (no. 14) in RTP, with a = 12.345(7) Å, b = 12.481(7) Å, c = 17.627(3) Å, β = 133.15(2) ° and V =1981.4 (1) Å^3. In HTP, the crystals are in the tetragonal non- centrosymmetric space group $P\text{-}42_1m$ (no. 113) and the detailed cell parameters are a = 8.8169(10) Å, b = 8.8169(10) Å, c = 6.4562(12) Å, and V =501.89(12) Å^3. Obviously, the unit cell parameters of **1** change abruptly and remarkably near the phase- transition temperature (Fig. S4) and the crystal volume in the HTP shows an approximately 4- fold decrease compared with that in the RTP. However, upon cooling or warming between the two temperatures, the crystals present no distinct, visual changes. In fact, what interests us is the crystallographic transition from RTP to HTP.

A change of spatial symmetric operations from $P2_1/c$ to $P\text{-}42_1m$ is depicted in Fig. 3. During the transition from the HTP to RTP symmetry breaking phenomenon happens and a total symmetry decrease from eight symmetric elements (E, $2S_4$, C_2,

$2C_2'$, $2\sigma_d$) to four symmetric elements (E, C_2, I, σ_h). In fact, an application of Landau theory to the phase transition was not necessarily sufficient evidence to indicate the presence of a second- order phase transition. Therefore, other properties should be measured to further confirm the character of the phase transition. The Curie symmetry principle tells us that the space group with broken symmetry of the RTP is a subgroup of the HTP, i.e., $P2_1/c$ is a subgroup of P-42m, in good agreement with macroscopic symmetry breaking.

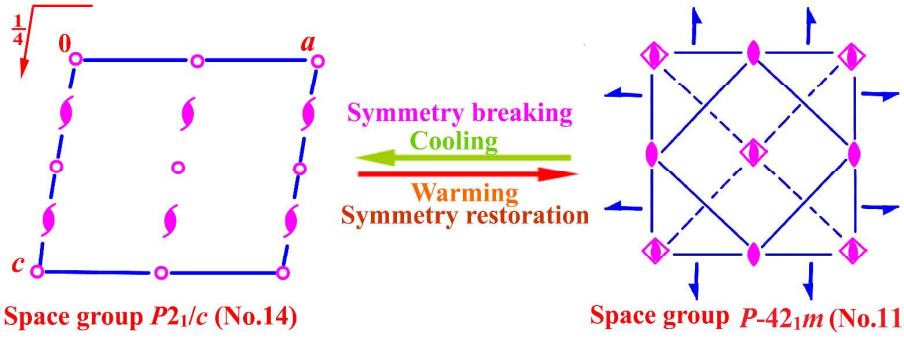

Fig. 3 Spatial symmetry operations change from RTP $P2_1/c$ to HTP ($P4/mbm$)

The key structural characteristic of **1** is the anionic $[Mn(HCOO)_3]^-$ cage enclosed by Mn-O-C-O-Mn units, within which the guest imidazolium cation resides (Fig. 4). It has been shown that the size of the charge balancing cations is the significant factor driving the crystallization of these frameworks and that may influence the apparent 'breathing' nature of the framework brought about by the abrupt change of the Mn-O-C angles and a much smaller change in the O-C-O angles.[18] For instance, the mean value of the Mn-O-C angles is 121.9° in $[CH_3NH_3]\cdot[Mn(HCOO)_3]$, 125.2° in $[CH_3CH_2NH_3]\cdot[Mn(HCOO)_3]$, 127.0° in $[(CH_3)_2NH_2]\cdot[Mn(HCOO)_3]$, and 128.7° in $[(CH_2)_3NH_2]\cdot[Mn(HCOO)_3]$. Due to the fact that the size of the imidazolium cation is larger than the mentioned alkylammonium, the averaged value of the Mn-O-C angles is 135.1° in the $[(C_3N_2H_5)]\cdot[Mn(HCOO)_3]$ (Table S1). Consequently, the volume of these cage compounds augment correspondingly with the increasing size of the cations.

A precise analysis of the main packing and structural differences between the RTP and HTP is needed to disclose the phase transition mechanism at 438.0 K. As shown in Fig. 4, six crystallographically independent $HCOO^-$ bridges in the RTP are ordered

whereas one of the two halves of crystallographically independent $HCOO^-$ in the HTP sways and blurs over four positions, as required by the tetragonal imposed symmetry. By and large, the $Mn(HCOO)_3^-$ cage exhibits high flexibility in a variety of symmetry elements, and its volume expands slightly from the RTP to the HTP. On the other hand, in the RTP two crystallographically independent imidazolium cations are totally frozen to be ordered, and each has a single orientation with the carbon and nitrogen atom definitely distinguishable. Besides it exists in the cavity of the formate framework, and three conventional N-H···O hydrogen bonds are formed with the three formate groups. Namely, for RTP, the imidazolium guest cation was fixed inside the formate cage through H-bonding interactions with the normal geometry. Contrarily, the molecular motions of the imidazolium cations in the HTP become more vigorous and are highly dynamically disordered, nearly over arbitrary orientation. Hence, the disordered tetragonally structural configuration was adopted for imidazolium cation, forming several N-H···O hydrogen bonds with the framework formate edges. As a result, the $HCOO^-$ edges and MnO_6 octahedra of one cube grid (Fig. 4(a) and Fig. 4(b)) also twist and rotate significantly to cater for the sway of the imidazolium cation (Table S1), for example, the MnO_6 octahedra rotate by approximately 30°. Overall, the host-guest interaction coupled with the synergic order- disorder transitions of the $Mn(HCOO)_3^-$ cage and the $[(C_3N_2H_5)]^+$ guest during the heating/ cooling process contribute to the crystal phase transition from RTP to HTP, which suggests that the mechanism of this phase transition is complicated, corresponding to the DSC analyses and with the heating process, the cage units per cell decrease from eight (in RTP) to two (HTP).

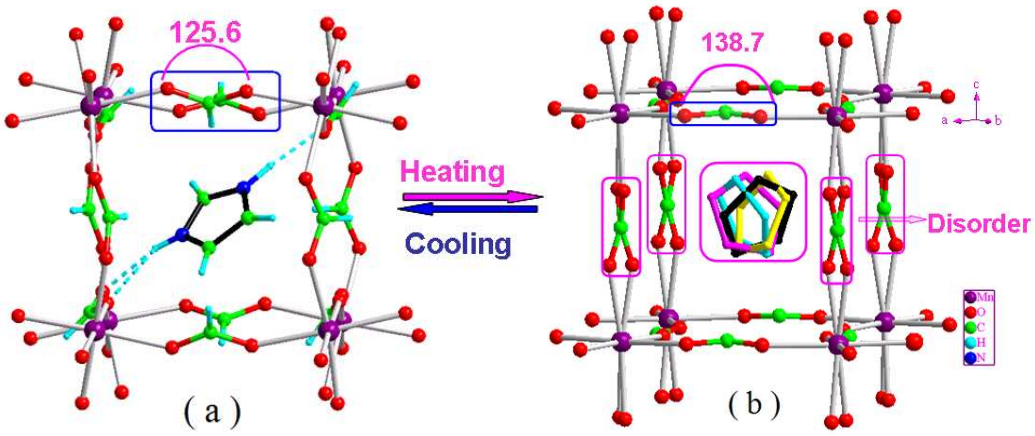

Fig. 4 The details of the abrupt order-disorder transform of imidazolium guests as well as the sway and the rotation of the cage-like framework are shown in (a) at 293 K (RTP) and (b) at 453 K (HTP, H atoms were omitted for clarity).

From a topological point of view, the Mn-formate framework with $4^{12}\cdot6^3$ topology is formed by one Mn connecting to its six neighbors through anti-anti formates in an octahedral arrangement (Fig. 5(a) and Fig. 5(c)). In the RTP, the void formed by four nearest-neighboring Mn atoms is a quadrilateral in the *bc* plane with Mn···Mn distances of 6.1787(36) and 6.4153(33) Å, while in the HTP, the void becomes rectangular in the *ab* plane with two distinct pairs of Mn···Mn distances (6.2345(5) and 6.4562(12) Å) (Fig. 5(b) and Fig. 5(d)). Besides, two Mn···Mn···Mn angles (91.8 and 91.7°) of the void in the RTP deviate greatly from that (90°) in the HTP, indicating that the relative locations of the Mn atoms alter obviously after the phase transition. Obviously, as the temperature rises from 293 K to 453 K, the $[Mn(HCOO)_3]^-$ cage shows high flexibility and its volume expands slightly, which will make the formate cage large enough to accommodate the disordered imidazolium cation. In a word, the structural differences among RTP and HTP can mainly be attributed to the sway or rotation of the $HCOO^-$ bridges and the imidazolium cation guest.

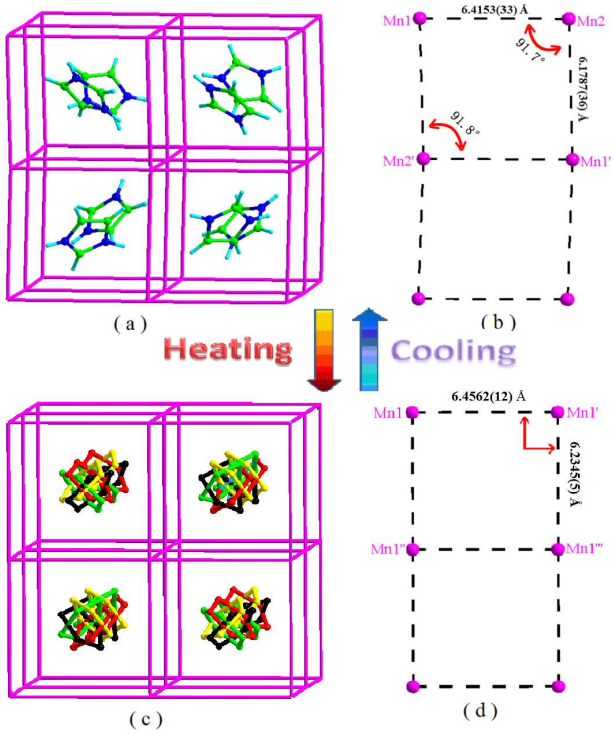

Fig. 5 The frameworks of **1** at (a) 293 K (RTP) and (c) 453 K (HTP) are in topological views. (b) Quadrilateral void formed by four nearest- neighboring Mn atoms at 293 K. (d) Rectangular void formed by four nearest- neighboring Mn atoms at 453 K.

The Mn^{2+} ion is octahedrally coordinated to six oxygen atoms of deprotonated formic acid moieties, all of which act as end-to-end bridging ligands between two Mn^{2+} ions, thus forming a three- dimensional cage- like framework (Fig. 6). There exist numerous hydrogen bonds with N-H···O distances in the range 2.792(4) – 3.26(3) Å (Table S2), which connect the imidazolium cations to the cages and further improve the stability of the 3D-framework. In a word, it is clear that these hydrogen bonds and other noncovalent interaction-static attracting forces, like Coulombic and van der Waals forces, tightly hold the anions and cations together and contribute to the formation of the 3D framework. However, the N-H···O hydrogen bonds and the packing diagrams between RTP and HTP are slightly different. The analysis of high T_c structural phase transition mentioned above is consistent with the DSC and the following dielectric measurements.

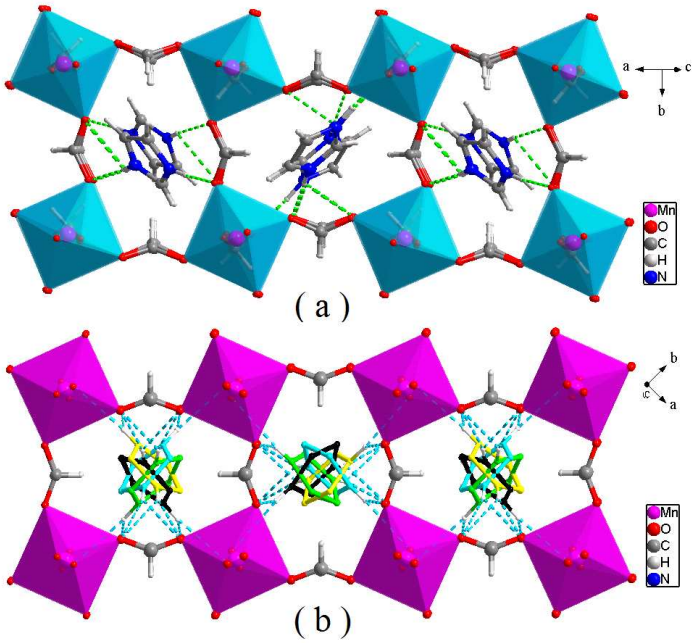

Fig. 6 View of the packing of **1**: (a) RTP at 293 K, (b) HTP at 453 K. Dashed line indicated hydrogen bonds.

Variable- temperature IR spectra.

As the temperature- dependent infrared spectroscopic investigations may shed more light on information about the possible participation of the imidazolium cations dynamics in the mechanism of the phase transition, we have undertaken the infrared studies on **1** in the wavenumber range between 4000 and 450 cm^{-1} at the selected temperatures (293- 463 K) covering the region of the phase transition (Fig S1). Based on the preceding literatures concerning the formate perovskite[16] and different imidazolium compounds,[35-36] the vibrational spectra of **1** may be comprehended unambiguously by dividing k =0 vibrations into internal vibrations of the imidazolium and formate ions, and the lattice vibrations.

As observed in the imidazolium halogenoantimonates (III) and bismuthates (III),[35] the changes of crucial importance in the positions and shapes of certain IR peaks of **1** are all caused by the stretching and bending vibrations of the imidazolium cations, suggesting that no obvious changes can be ascribed to the formate anions (Fig. 7, Fig. S5). Obviously, this behavior proves that the phase transition in $(C_3N_2H_5)\cdot[Mn(HCOO)_3]$ has an order-disorder character and is governed by dynamics

of the imidazolium cations. In detail, the changes in the Fig. 7(b) are aroused by the deformations of the N-H bonds δ (N-H) and of the whole ring δ(R) while those in the Fig. 7(c) are evoked by the deformation of the carbon- hydrogen bonds δ (C- H). It is worth noting, however, that the deformation of the modes δ (N-H), δ(R) and δ (C-H) are observed as broad lines close to room temperature while at high temperature they appear as broader and less intense and usually shift toward the lower frequencies.

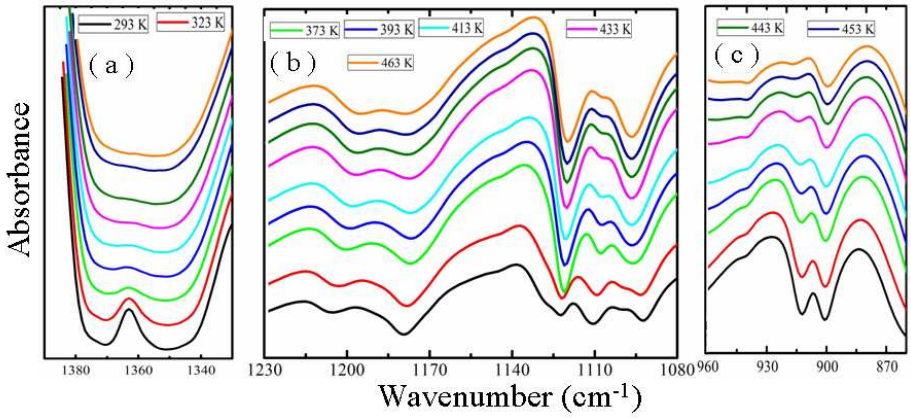

Fig. 7 Detail of the IR spectra corresponding to the spectral ranges 1330-1390, 1080-1230, and 860-960 cm^{-1} ((a), (b), (c)) recorded at different temperatures in the interval [293-463] K.

Temperature-dependent IR studies evince when temperatures decrease below T_c, many of the IR bands split into a few components (Fig 7(a)). Besides, when the temperature increases, there form more H-bonds, which will reduce that the stretching modes usually shift toward lower frequencies and that the corresponding bands become broader.[37-38] With increasing strength of the H-bonds, the out-of-plane rocking mode should show increase in frequency, which is in marked contrast to the stretching mode. Furthermore, the analysis of the temperature dependence of splitting for IR bands exhibits that splitting of these bands increase continuously below T_c, without any distinct jump at T_c, which completely indicates that the phase transition is a second-order one. In conclusion, the continuous nature of the transition is well reflected in the variable-temperature infrared spectra, which is consistent with the DSC and the single crystal X-ray analysis.

Dielectric properties.

Usually, the physical properties, such as the dielectric constant (both real part ε′ and dielectric loss) will exhibit sharp changes near the phase-transition point and the magnitude of the changes will also be relative to the characteristics of the phase transitions. Therefore, the high T_c dielectric properties of **1** were confirmed through variable-temperature dielectric measurements, and figure 8 shows the real parts (ε′) and dielectric losses (tan δ) of the dielectric permittivities obtained at different frequencies on heating.

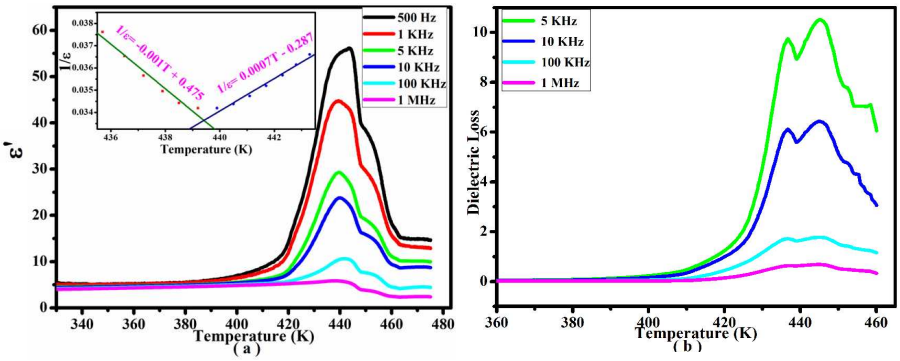

Fig. 8 (a) Real parts ε′ of the dielectric permittivities of **1** measured on powdered sample at selected frequencies on heating. Inset: Plot of 1/ε′ vs. temperature (the frequency is fixed at 5 KHz). (b) Dielectric losses (tan δ) as the function of temperature measured at fixed frequencies of 5K Hz, 10K Hz, 100 K Hz and 1 M Hz are presented upon the heating process.

As illustrated in Fig. 8(a), the real part (ε′) of the dielectric constant distinctly experiences a wide dielectric transition in the temperature interval of 410- 460 K. As for details, it almost remains unchanged at about 5-6 below the T_c but displays a progressive and clear augment of one order of magnitude between 410 and 460 K(up to 60 at 500 Hz), especially showing a strong frequency dependence and a prominent change up to approximately 438.1 K. Indeed, the maximum ε′ values vary strongly with the frequency and are up to six times at lowest frequency than those at highest frequency, which is the characteristic feature for the phase transition. It is very interesting to note that the real part (ε′) displays a broad peak at 438.1 K at 1 MHz,

which is treated as an extremely effective indicator of the structural phase transition, corresponding well with the phase transition temperature determined by DSC. The changes of the ε' values may be associated to the molecular motions of the imidazolium cations and the framework. In the HTP, the orientationally disordered imidazolium cations may get enough energy to be able to obey the alteration in the external electric field more easily, which enhances their contribution to the polarization in return, generating an increase in dielectric permittivity.[39]

Because the imidazolium cations transform from order to disorder and the cage-like framework sway and rotate, **1** [28-29] exhibits structural phase transition with T_c high close to 438 K, coupled with giant dielectric anomalies. Remarkably, the compound that displays dielectric transition at such a high T_c is comparatively rare and AMFFs usually exhibit low T_c, as previously reported. As it is, the high phase transition temperature can match with those of a typical inorganic ceramic ferroelectric $BaTiO_3$ (T_c = 393 K)[30] and some molecular ferroelectrics, such as triglycine fluoberyllate (TGFB, T_c = 352 K).[33]

Corresponding with the dielectric constants, the dielectric losses, measured at fixed 5 KHz, 10 KHz, 100 KHz and 1 MHz, also exhibit an obvious alteration and show no significant dielectric relaxation at different frequencies in the heating process (Fig. 8 (b)). In the measured temperature ranges, the dielectric anomalies are observed, being well coincident with that of DSC and further suggesting that there may be the occurrence of a reversible phase transition in the temperature window of 410 K to 460 K. The data are fitted with the Curie-Weiss law (Inset), $1/\varepsilon' \approx (T - T_0)/C$ where ε' is the real part of the dielectric constant, C is the Curie constant, T is the temperature, and T_0 is the Curie-Weiss temperature. According to the two equations of $1/\varepsilon$ = -0.001T + 0.475 and $1/\varepsilon$ =0.0007T – 0.287, the values of C_1 and C_2 are calculated to be 1000 and 1429, respectively. The ratio of C_2 / C_1 is estimated to be 1.4 and <4, indicating that it may be of second-order phase transition.

Besides, the frequency dependences of the real parts (ε') and dielectric losses (tan δ) of the dielectric permittivities at several temperatures are shown in Fig. 9(a) and Fig. 9(b), respectively. It is obvious that the magnitude of ε' and tan δ decrease with the

increasing frequency but increase with the augment of the temperature, which indicates the conductivity of **1**. Remarkably, the dielectric constants measured at different frequencies (1K Hz to 1 MHz) exhibit a frequency-independent property and there is no distinct dielectric relaxation process in the close vicinity of the transition temperature, confirming a relatively fast dipolar motion. Such high T_c and dielectric characteristics make **1** to be a useful high-T_c intelligent dielectric in capacitors for electric energy storage, molecule-based dielectric materials, and smart devices.

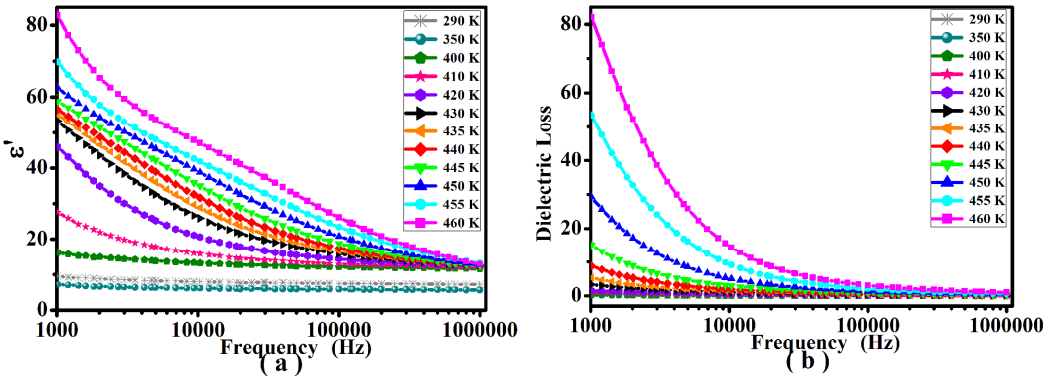

Fig. 9(a) Frequency dependences of the real parts of the dielectric permittivities of **1** obtained at various temperatures. Fig. 9(b) Frequency dependences of the dielectric losses (tan δ) of **1** measured at various temperatures.

Conclusion

In conclusion, one dielectric compound $(C_3N_2H_5)\cdot[Mn(HCOO)_3]$ with the perovskite architecture, showing extremely high phase transition temperature (high T_c) and prominent dielectric anomaly, was systematically characterized by a variety of means. It exhibits an abrupt structural phase transition at approximately 438 K, the highest T_c reported so far for formate series perovskite-like dielectric materials, the temperature at which the prominent dielectric anomalies occur. The structural phase transition involves a symmetry change from RTP in $P2_1/c$ to HTP in $P\text{-}42_1m$, owing to the abrupt order-disorder transform of imidazolium cation in the cavity and a subsequent successive displacement and large rotation for both the $HCOO^-$ groups and the octahedraon- like MnO_6, which is conformed by temperature-dependent single crystal X- ray diffraction. Compound **1** stands for a new class of extremely

high-temperature molecular dielectrics which display striking dielectric anomalies. Investigations on such system can illuminate deeply the understanding of structural phase transitions of molecular dielectrics and furnish an available tactic in seeking for new electric ordering materials. Emphatically, the present work has successfully demonstrated that **1** is an extremely promising candidate for the design and synthesis of molecular-based dielectrics with high phase transition temperature and it may open a new avenue for the potential applications in sensing, dielectric devices, energy storage, data storage and molecular or flexible multifunctional electronic devices. A particular study is now underway.

Acknowledgements

This work was financially supported by the Project 973 (No. 2014CB848800), the National Natural Science Foundation of China (Nos. 21422101, 21301029), Jiangsu Province NSF (Nos. BK20130600, BK20140056), Program for NCET and SRFDP (20130092120013).

Supporting Information Available

Supplementary figures S1−S5 and tables S1-S2 for this article are available in Supporting Information. Supplementary crystallographic data are available from the Cambridge Crystallographic Data Centre, with CCDC No. 1057529 for RTP, and No. 1057530 for HTP. Copies of these data can be obtained free of charge from the Cambridge Crystallographic Data Centre, 12 Union Road, Cambridge CB2 1EZ, UK; fax: (+44) 1223-336-033; or e-mail: deposit@ccdc.cam.ac.uk. This information is available free of charge via the Internet at http://pubs.acs.org/.

References

1 G. Rogez, N. Viart and M. Drillon, *Angew. Chem., Int. Ed.*, 2010, **49**, 1921-1923.

2 R. Ramesh, *Nature*, 2009, **461**, 1218-1219.

3 W. Zhang and R. G. Xiong, *Chem. Rev.*, 2012, **112**, 1163-1195.

4 D. W. Fu, H. L. Cai, Y. Liu, Q. Ye, W. Zhang, Y. Zhang, X. Y. Chen, G. Giovannetti, M. Capone, J. Li and R.G. Xiong, *Science*, 2013, **339**, 425-428.

5 I. E. Collings, A. B. Cairns, A. L. Thompson, J. E. Parker, C. C. Tang, M. G. Tucker, J. Catafesta, C. Levelut, J. Haines, V. Dmitriev, P. Pattison and A. L. Goodwin, *J. Am. Chem. Soc.*, 2013, **135**, 7610-7620.

6 A. Coskun, M. Banaszak, R. D. Astumian, J. F. Stoddart and B. A. Grzybowski, *Chem. Soc. Rev.*, 2012, **41**, 19-30.

7 P. P. Shi, Q. Ye, Q. Li, H. T. Wang, D. W. Fu, Y. Zhang and R. G. Xiong, *Chem. Mater.*, 2014, **26**, 6042-6049.

8 D. W. Fu, W. Zhang, H. L. Cai, Y. Zhang, R. G. Xiong, S. D. Huang and T. Nakamura, *Angew. Chem. Int. Ed.*, 2011, **50**, 11947-11951.

9 P. Zhou, Z. H. Sun, S. Q. Zhang, C. M. Ji, S. G. Zhao, R. G. Xiong and J. H. Luo, *J. Mater. Chem.* C, 2014, **2**, 2341-2345.

10 Z. Y. Du, Y. P. Zhao, W. X. Zhang, H. L. Zhou, C. T. He, W. Xue, B. Y. Wang and X. M. Chen, *Chem. Commun.*, 2014, **50**, 1989-1991.

11 Z. Y. Du, Y. P. Zhao, C. T. He, B. Y. Wang, W. Xue, H. L. Zhou, J. Bai, B. Huang, W. X. Zhang and X. M. Chen, *Crystal. Growth Des.*, 2014, **14**, 3903-3909.

12 Z. M. Wang, B. Zhang, T. Otsuka, K. Inoue, H. Kobayashi and M. Kurmood, *Dalton Trans.*, 2004, 2209-2216.

13 M. Maczka, A. Pietraszko, B. Macalik and K. Hermanowicz, *Inorg. Chem.*, 2014, **53**, 787-794.

14 Q. Q. Zhu, R. Shang, S. Chen, C. L. Liu, Z. M. Wang and S. Gao, *Inorg. Chem.*, 2014, **53**, 8708-8716.

15 M. Maczka, A. Gagor, B. Macalik, A. Pikul, M. Pttak and J. Hanuza, *Inorg. Chem.*, 2014, **53**, 457-467.

16 M. Sanchez- Andujar, L. C. Gomez- Aguirre, B. P. Doldan, S. Yanez-Vilar, R. Artiaga, A. L. Llamas-Saiz, R. S. Manna, F. Schnelle, M. Lang and F. Ritter, *CrystEngComm.*, 2014, **16**, 3558-3566.

17 B. Pato- Doldan, M. Sanchez- Andujar, L. C. Gomez- Aguirre, S. Yanez- Vilar, J. Lopez- Beceiro, C. Gracia- Fernandez, A. A. Haghighirad, F. Ritter, S. Castro-Garcia and M. A. Senaris- Rodriguez, *Phy. Chem. Chem.* Phys., 2012, **14**, 8498-8501.

18 R. Shang, G. C. Xu, Z. M. Wang and S. Gao, *Chem. Eur. J.*, 2014, **20**, 1146-1158.

19 Z. H. Sun, T. L. Chen, J. H. Luo and M. C. Hong, *Angew. Chem. Int. Ed.*, 2012, **51**, 3871-3876.

20 M. Weclawik, A. Gagor, A. Piecha, R. Jakubas and W. Medycki, *CrystEngComm.*, 2013, **15**, 5633-5640.

21 Z. H. Sun, S. H. Li, S. Q. Zhang, F. Deng, M. C. Hong and J. H. Luo, *Adv. Opt. Mater.*, 2014, **2**, 1199-1205.

22 Y. Zhang, H. Y. Ye, H. L. Cai, D. W. Fu, Q. Ye, W. Zhang, Q. H. Zhou, J. L. Wang, G. L. Yuan and R. G. Xiong, *Adv. Mater.*, 2014, **26**, 4515-4520.

23 D. W. Fu, W. Zhang, H. L. Cai, Y, Zhang, J. Z. Ge, R. G. Xiong and S. D. Huang, *J. Am. Chem. Soc.*, 2011, **133**, 12780-12786.

24 Y. Zhang, Y. M. Liu, H. Y. Ye, D. W. Fu, W. X. Gao, H. Ma, Z. G. Liu, Y. Y. Liu, W. Zhang, J. Y. Li, G. L. Yuan and R. G. Xiong, *Angew. Chem. Int. Ed.*, 2014, **53**, 5064-5068.

25 H. Y. Ye, S. H. Li, Y. Zhang, L. Zhou, F. Deng and R. G. Xiong, *J. Am. Chem. Soc.*, 2014, **136**, 10033-10040.

26 T. Akutagawa, H. Koshinaka, D. Sato, S. Tekeda, S.-I. Noro, H. Takahashi, R. Kumai, Y. Tokura and T. Nakamura, *Nat. Mater.*, 2009, **8**, 342-347.

27 D. W. Fu, H. L. Cai, S. H. Li, Q. Ye, L. Zhou, W. Zhang, Y. Zhang, F. Deng and R. G. Xiong, *Phy. Rev. Lett.*, 2013, **110**, 257601.

28 B. Q. Wang, H. B. Yan, Z. Q. Huang and Z. Zhang, *Acta Crystallogr. Sect. C: Crystal. Struct. Commum.*, 2013, **69**, 616-+.

29 B. Pato- Doldan, L. C. Gomez- Aguirre, J. M. Bermudez-Garcia, M.

Sanchez-Audujar, A. Fondado, J. Mira, S. Castro-Garcia and M. A. Senaris-Rodriguez, *RSC adv.*, 2013, **3**, 22404-22411.

30 J. Valasek, *Phys. Rev.*, 1921, **17**, 475-481.

31 A. Katrusiak and M. Szafranski, *Phys. Rev. Lett.*, 1999, **82**, 576-579.

32 A. Katrusiak, M. Szafranski and G. J. Mclntyre, *Phys. Rev. Lett.*, 2002, **89**, 215507.

33 T. Mitsui, I. Tatsuzaki and E. Nakamura, *An introduction to the physics of ferroelectrics*, Gorden and Breach Science Publishers, New York, 1976.

34 D. W. Fu, W. Zhang, H. L. Cai, J. Z. Ge, Y. Zhang and R. G. Xiong, *Adv. Mater.*, 2011, **23**, 5658-5662.

35 A. Piecha, R. Jakubas, G. Bator and J. Baran, *Vib. Spectrosc.*, 2009, **51**, 226-237.

36 A. Piecha, R. Jakubas, A. Pietraszko, J. Baran, W. Medycki and D. Kruk, *J. Solid State Chem.*, 2009, **182**, 2949-2960.

37 S. Jarmelo, I. Reva, P. R. Carey and R. Fausto, *Vib. Spectrosc.*, 2007, **43**, 395-404.

38 L. Sobczky, M. Obrzud and A. Filarowski, Molecules, 2013, **18**, 4467-4476.

39 S. Hajlaoui, I. Chaabane, A. Oueslati and K. Guidara, *Solid. State. Sci.*, 2013, **25**, 134-142.

A prominent dielectric material with extremely high-temperature and reversible phase transition in the high thermally stable perovskite-like architecture

Fang-Fang Wang, Cheng Chen, Yi Zhang, Heng-Yun Ye, Qiong Ye*, Da-Wei Fu*

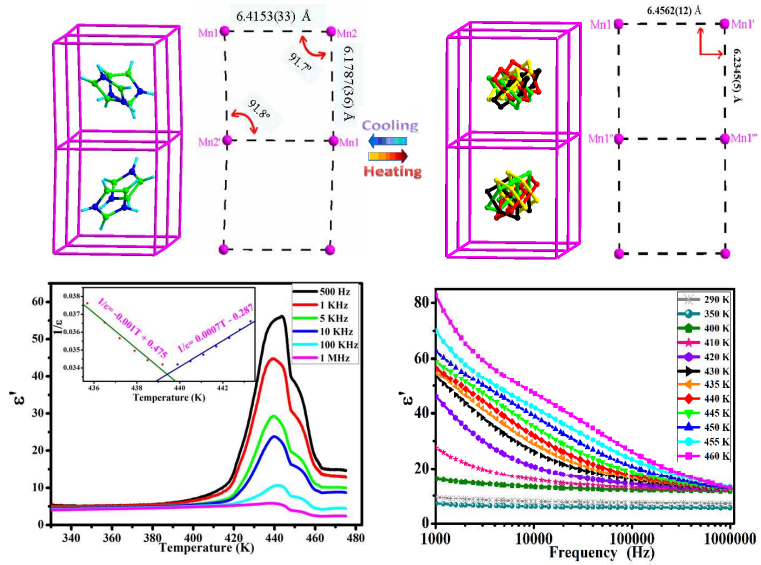

*E-mail: dawei@seu.edu.cn, yeqiong@seu.edu.cn